Springer

KSME

Journal of Mechanical Science and Technology 29 (2) (2015) 507~515
www.springerlink.com/content/1738-494x
DOI 10.1007/s12206-015-0111-4

Numerical investigation on the dynamic behaviors of turbine valve disc–seat impact at low velocity †

Jianfeng Mao[1,2,3], Weizhe Wang[1,2,*], Junhui Zhang[4] and Yingzheng Liu[1,2]

[1]*Key Lab of Education Ministry for Power Machinery and Engineering, Shanghai Jiao Tong University, Shanghai 200240, China*
[2]*Gas Turbine Research Institute, Shanghai Jiao Tong University, Shanghai 200240, China*
[3]*College of Mechanical Engineering, Zhejiang University of Technology, Hangzhou 310014, China*
[4]*Design & Research Institute, Shanghai Electric Power Generation Equipment Co., Ltd. Shanghai Turbine Plant, Shanghai 200240, China*

(Manuscript Received June 2, 2014; Revised October 4, 2014; Accepted November 6, 2014)

Abstract

In this study, the dynamic behaviors on a valve seat subjected to the impact of the valve disc at low velocities were investigated by using numerical analysis with finite element method. The impact damage of the valve disc against seat was evaluated through a three-dimensional dynamic explicit calculation. The parameters considered in the simulations were impact velocity, disc obliquity, aspect ratio, and contact area ratio. The model for impact calculation was implemented in the code ABAQUS, which is based on the constitutive equation and fracture strain equation of Johnson and Cook, as well as on continuum damage mechanics. The distribution of damage caused by the impact was computed and discussed. The impact damage of the valve disc was minimized when the disc obliquity was approximately 40°. The effects of variation of selected design parameters on dynamic behaviors were discussed. The best design parameters were proposed, which served as a guide for future valve design.

Keywords: Continuum damage mechanics; Finite element; Impact; Turbine valve

1. Introduction

The steam valve, which is composed of the stop and control valves, is widely used to adjust steam flow into the steam turbine. In addition to controlling steam flow, the stop valve is designed with a quick-shutdown capability to protect the steam turbine from emergency malfunction. However, instant impact is generated between the valve seat and the valve disc when the stop valve is shut down quickly (Fig. 2). This condition seriously damages the components, which significantly decreases the life span of the steam valve. Accordingly, a numerical investigation on the dynamic behavior of the steam valve subjected to the instant impact between the valve disc and the valve seat is highly desirable to improve the structural design of the steam valve.

Numerous efforts have been made to investigate the impact damage between the valve disc and the valve seat. In 1987, S. K. Dawawala [1] reported on the instant impact between the valve disc and the valve seat during the process of quickly shutting down the stop valve. The damage caused by the instant impact significantly influenced the life span of the steam valve. A further study by Robert Swanekamp [2] illustrated the most serious impact damage, which reduced the life span of the valve to three months. Thus, Mazur et al. [3] numerically studied the solid particle impact of the turbine main stop valve by using the commercial software ANASYS. They determined that the impact process strongly depends on the impact trajectories and angle of impact. Z. B. Chen [4] analyzed the transient temperature and stress variations of the valve casing by using finite element method to predict the fatigue behaviors of control valves on the intermediate-pressure section of steam turbine. In addition, a further study on the transient temperature and stress distributions on three-dimensional (3D) configure of control valve of steam turbine was conducted by Peng et al. [5]. As previously discussed, the impact damage was not considered in the investigation. The instant impact caused by the quick closing of the turbine stop valve results in a serious damage on the valve seat, which induces the failure of the steam valve. Furthermore, high energy impact damage tolerance [6] was proposed to guide the design of steam valve. Borvik et al. [7] performed experimental and numerical investigation on the impact of steel plates with blunt nose projectiles. They used a finite element (FE) model and predicted the influence of material, temperature, and strain rate on the impact damage. Additionally, Bonoral [8] and Chandrakanth [9] proposed functions to illustrate the impact damage potential. However, the material parameters used in

*Corresponding author. Tel.: +86 21 34205986, Fax.: +86 21 34206719
E-mail address: wangwz0214@sjtu.edu.cn
† Recommended by Associate Editor In-Ha Sung

these functions needed to be determined by a large number of experimental data. This setback hindered wide applications in the engineering field. In addition, some efforts were made to simplify these functions by studying the parametric sensitivity. Corbett et al. [10] studied the influence of non-normal impact into projectile–target configurations. They developed the numerical codes that can predict local deformation, local failure, and target response reasonably accurately. Furthermore, Goldsmith and Finnegan [11] performed experiments to study the influence of material, thickness, initial projectile velocity, and angle of incidence on the target response. Most of the aforementioned studies focused on experimental samples with simplified geometries to investigate the impact damage. However, few studies were performed to investigate quantitatively the damage caused by the instant impact to the real steam valves during the process of quick shutting down of the stop valve. Thus, the numerical analysis of the instant impact for the real steam valve under the condition of the quick closing of the stop valve is highly desirable to improve the design of the valve disc and valve seat.

The major objective of this study is to investigate numerically the instant impact damage in a real steam valve. Thus, a stop valve of 1000 MW ultra-supercritical power unit, including the valve casing, the valve disc, and the valve seat, was chosen for the study. Therefore, a numerical model of the stop valve was established by using FEA. A viscoplasticity model was used to calculate the stress–strain behaviors of the stop valve, and a model based on the damage evolution law was adopted to analyze the instant impact damage during the quick closing of the stop valve. The influence of the instant impact on the stop valve was investigated in terms of stress, strain, damage, and geometries.

2. Mathematical model

2.1 Damage evolution theory

In the calculation, the damage approach by Lemaitre [12] was adopted to investigate the instant impact damage, and the expression is presented as follows:

$$\dot{D} = \frac{\partial F_D\left(Y, p, D, ...\right)}{\partial Y} \dot{p} \cdot \left(1 - D\right) \tag{1}$$

where $\dot{D}$ is the growth rate of damage parameter, p is the accumulated plastic strain, $\dot{p}$ is plastic strain rate, and D is the damage parameter (simplified as "damage"). In addition, Y in Eq. (1) is the strain energy per volume unit and is defined as Eq. (2) [13]:

$$\begin{aligned} Y &= \frac{\left(3/2\right)\sigma_{ij}{}^{D}\sigma_{ij}{}^{D}}{2E\left(1-D\right)^2}\left[\frac{2}{3}\left(1+\nu\right)+3\left(1-2\nu\right)\left(\frac{\sigma_H}{\sigma_{eq}}\right)^2\right] \\ &= \frac{\sigma_{eq}{}^2}{2E\left(1-D\right)^2}R_v = \frac{\tilde{\sigma}_{eq}{}^2}{2E}R_v \end{aligned} \tag{2}$$

where σ_{eq} is the Von Mises equivalent stress, R_v is the triaxiality function, and $\tilde{\sigma}_{eq}$ is the damage effective stress, which are given as follows:

$$\begin{aligned} &\sigma_{eq} = \left(\tfrac{2}{3}\sigma_{ij}{}^{D}\sigma_{ij}{}^{D}\right)^{1/2} \\ &R_v = \tfrac{2}{3}\left(1+\nu\right)+3\left(1-2\nu\right)\left(\sigma_H/\sigma_{eq}\right)^2 \\ &\tilde{\sigma}_{eq} = \sigma_{eq}/\left(1-D\right). \end{aligned} \tag{3}$$

F_D in Eq. (1) is a damage potential function, which was given by Lemaitre [14] to determine the damage behavior under the impact loadings. In addition, the expression of the damage potential function was defined as follows:

$$F_D = \frac{Y^2}{2S\left(1-D\right)}\frac{\left(D_{cr}-D\right)^{\alpha-1/\alpha}}{p^{2+n/n}} \tag{4}$$

where S is a material constant associated with the damage energy strength, α is the material damage exponent, n is the material hardening exponent, and p is the accumulated plastic strain. Subsequently, the damage evolution law can be obtained by substituting Eqs. (2)-(4) into Eq. (1),

$$dD = \begin{cases} \alpha\dfrac{\left(D_{cr}-D_0\right)^{1/\alpha}}{\ln p_f - \ln p_{th}}R_v\left(D_{cr}-D\right)^{\alpha-1/\alpha}\dfrac{dp}{p} & p \ge p_{th} \\ 0 & p < p_{th} \end{cases} \tag{5}$$

where p_{th} is the threshold value of accumulated plastic strain, D_0 is the initial damage of the material, and D_{cr} is the critical damage to determine the failure of the stop valve. R_v is always larger than 1 because of the effect of the multiaxial stress. According to Eq. (5), the stress triaxiality can accelerate the evolution of the damage parameter D to some extent. In the Johnson and Cook (1985) fracture strain model [14], the actual value of the fracture strain was expressed as the products of variable terms of stress triaxiality, strain rate, and temperature. The following is a modified version of Johnson–Cook (J–C) fracture strain model:

$$p_f = \left[D_1 + D_2\exp\left(D_3\sigma^*\right)\right]\left[1+\dot{p}\right]^{D_4}\left[1+D_5T^*\right] \tag{6}$$

where the stress triaxiality ratio is defined as $\sigma^* = \sigma_H/\sigma_{eq}$, σ_H is the hydrostatic stress, D_1 to D_5 are material constants, $\dot{p}$ is plastic strain rate, T^* is the homologous temperature defined as $T^* = \left(T-T_0\right)/\left(T_m-T_0\right)$, T is the absolute temperature, T_0 is the room temperature, and T_m is the melting temperature of the material. Isotropic plasticity coupled with damage under a Von Mises yield criterion leads to the following expression for the plastic potential:

$$F_p = f\left(\tilde{\sigma}\right) - \sigma_y\left(T\right) - R(p,T) \le 0 \tag{7}$$

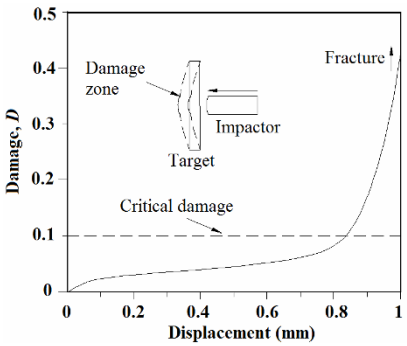

Fig. 1. Impact damage vs. displacement to illustrate the critical and fracture points.

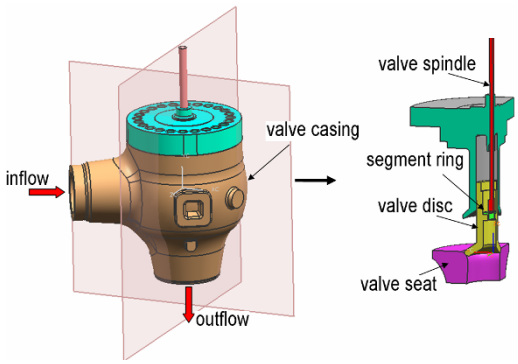

Fig. 2. Outer and internal structure of the turbine valve.

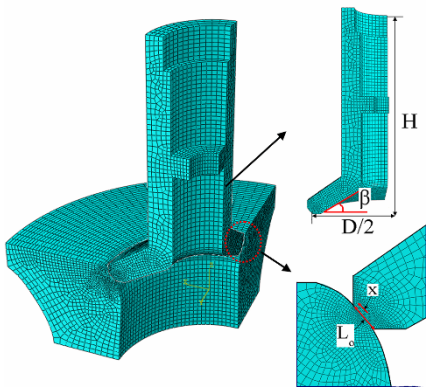

Fig. 3. FE mesh of the valve disc and seat.

where $f(\cdot)$ is a convex function to define the equivalent stress, σ_y is the yield strength, R is the strain hardening function, and T is the temperature. Subsequently, the relation between the equivalent stress and the damage was established by using Eq. (8) to investigate the influence of the instant impact damage on the stress behavior ([15-17]).

$$\sigma_{eq} = \left[1-D\right]\left[A+Br^{\kappa}\right]\left[1+\dot{r}^{*}\right]^{C}\left[1-T^{*m}\right] \tag{8}$$

where A, B, C, κ, and m are material constants, r is the damage accumulated plastic strain defined as $\dot{r} = (1-D)\dot{p}$, $\dot{r}^{*} = \dot{r}/\dot{r}_0$ is a dimensionless strain rate, and $\dot{r}_0$ is a reference strain rate. Eqs. (1) and (8) involve the assumption that $D = 0$ for a virgin material and that fracture occurs when $D = 1$. As previously mentioned, the critical damage D_{cr} is set to 0.1 in Table 1, and the physical proof for identification of which is demonstrated in Fig. 1. The damage significantly increases up to fracture after critical damage. Thus, in most cases, the critical damage is regarded as failure point because of the subsequent potential danger to fracture.

In addition, according to the adiabatic assumption [18], the plastic work associated with plastic deformation of the configuration during the instant impact between the valve disc and the valve seat was converted into heat, which was absorbed by the material. Furthermore, the outside of the valve casing was set to the adiabatic boundary. When the softening caused by damage and temperature exceeds the strain and strain rate hardening during the impact process, the adiabatic temperature was expected to concentrate on the impact zone [19]. The adiabatic temperature rise can be expressed as follows:

$$\Delta T = \frac{\eta}{\rho c_p}\int_0^{\varepsilon}\sigma(p)dp \tag{9}$$

where c_p and η are the specific heat and the fraction of plastic work converted into heat, respectively, and ρ is the material density, ε is the strain. Given that 9Cr–1Mo steel is widely used in coal-fired power plant, the experimental data are available in many literatures, such as Samantaray et al. [20], S. R. Chen [21], and Lemaitre et al. [22], I. Rohr [23]. The database of mechanical properties is provided by our manufacturer on specific material. The material parameters for 9Cr–1Mo steel presented in Table 1 are obtained by using least squares regression, some of which are similar to the material parameters in the preceding literature.

2.2 FE model

A stop valve of a 1000 MW ultra-supercritical power unit is shown in Fig. 2, which includes valve casing, valve spindle, segment ring, valve disc, and valve seat. As an impactor source, the upper end of the valve spindle was mounted to hydraulic drive cylinder and spring system, whereas the lower end was connected to the valve disc. Although the dynamic behavior was quite complicated for the system, the instant velocity can be easily detected immediately before the impact. Therefore, the initial impact velocity was selected as a boundary condition. A comparison of the mass of the spindle and that of the disc revealed that the former was significantly light, and it was thus neglected in the calculation. Accordingly, the simplified FE model of the disc and seat was established, as illustrated in Fig. 3. The mesh density is also displayed in Fig. 3. The calculation of the instant impact between the valve disc

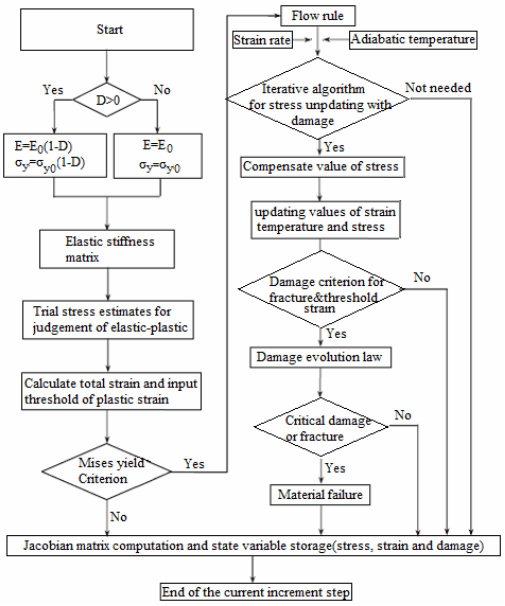

Fig. 4. Flowchart of coupled calculation of stresses with damage evolution.

and the valve seat was performed by using commercial FE package ABAQUS. The J–C equivalent stress was calculated with user-defined program that can be achieved by modifying default constitutive equations in ABAQUS. The newly developed J-C stress equation is different from the default equation regarding the damage parameter. The damage calculation method was considered as fully coupled method in our program.

The flowchart of the coupled calculation of stresses with damage evolution is presented in Fig. 4 to clarify further the FE procedure. The total computational elements for the stop valve are 178840, and the mesh type is eight-node 3D solid elements. During the process of the instant impact, the time step was set to 10^{-6} for the simulation. The sensitivity of the simulation results to the element density and the time step was checked by repeating calculations with different number of cells and time steps. The elements and time step in this work were determined to yield satisfactory results. In addition, the stop valve was made of 9Cr–1Mo, and the material parameters for the damage model are listed in Table 1.

3. Results and discussion

In this study, the influence of the instant impact between the valve disc and the valve seat on the damage of the stop valve was investigated by changing valve disc obliquity β, contact area ratio δ, aspect ratio H/D, and impact velocity. The detailed information is listed in Table 2. In addition, the filter circulating around the valve disc maintained the uniform steam pressure distribution on the valve disc in the circumferential direction as steam flowed through the valve. Accordingly, the influence of the steam pressure on the valve disc was neglected in this study.

Table 1. Material parameters for 9Cr–1Mo in the simulations.

Elastic constants & density			Yield stress & strain hardening		
E (GPa)	ν	ρ (kg/m^3)	A (MPa)	B (MPa)	κ
220	0.3	7680	122	225	0.12

Adiabatic heating & temperature softening					
C_p (J/kg.k)	η	λ (1/K)	T_m (K)	T_0 (K)	m
452	0.5	1.1×10^{-5}	1803	293	0.541

Damage evolution				Strain rate hardening	
D_{cr}	α	p_{th}	n	$\dot{p}_0, \dot{r}_0$ (1/s)	C
0.1	0.198	0.202	0.14	1	0.105

Fracture strain constants					Initial damage
D_1	D_2	D_3	D_4	D_5	D_0
0.0705	1.732	−0.54	−0.015	0	0

Table 2. Design parameters in the simulations.

Predefined parameters	N = 3 m/s, δ = 0.8, H/D = 1		
Disc obliquity β	30°	40°	60°
Predefined parameters	v = 3 m/s, β = 40°, H/D = 1		
Contact area ratio δ	0.4	0.6	0.8
Predefined parameters	v = 3 m/s, β = 40°, δ = 0.8		
Aspect ratio H/D	H/D = 1.26	H/D = 1	H/D = 0.72
Predefined parameters	B = 40°, δ = 0.8, H/D = 1		
Impact velocity v	1 m/s	3 m/s	6 m/s

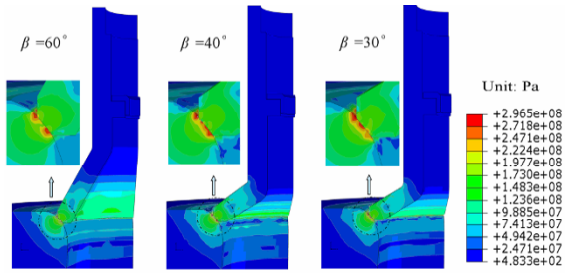

Fig. 5. Distribution of equivalent stress for different disc obliquity with v = 3 m/s.

3.1 Effect of the valve disc obliquity

The effect of the valve disc obliquity on the stop valve was investigated in terms of β = 30°, 40°, and 60° under the fixed impact velocity 3 m/s and the aspect ratio H/D = 1. The calculated J–C equivalent stress (see Ref. [8]) distributions in the valve disc and the valve seat at transient time 0.05 ms are shown in Fig. 5. Fig. 5 illustrates that the maximum σ_{eq} concentrated in the circular area and distributed in the valve seat. Furthermore, the increasing β led to the decreased contact area and promoted maximum σ_{eq} to move toward both ends of the contact area at β = 60°. In addition, comparing the maximum σ_{eq} distribution at the contact area among β = 30°, 40° and 60° indicated that this distribution is the most homogeneous for the valve disc obliquity β = 40°.

Subsequently, the residual velocity for β = 30°, 40°, and 60°

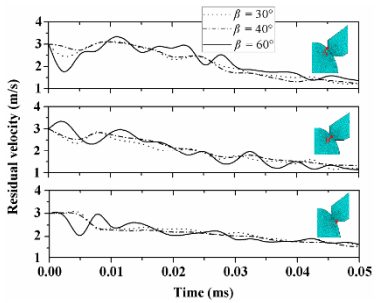

Fig. 6. Residual velocity vs. time for different disc obliquity at typical points.

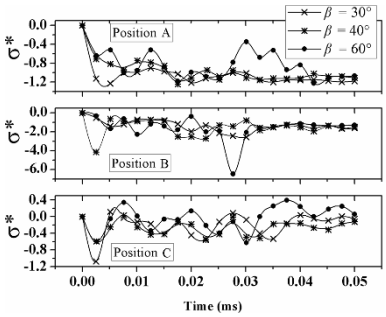

Fig. 7. Triaxiality factor changes with time for different disc obliquity at three positions.

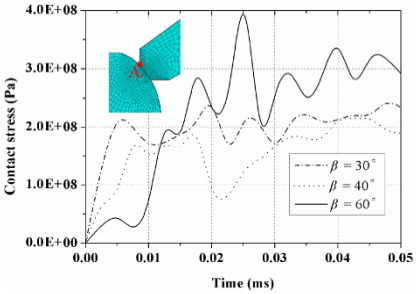

Fig. 8. Effect of disc obliquity on the contact stress–time history plot at the position of significant damage.

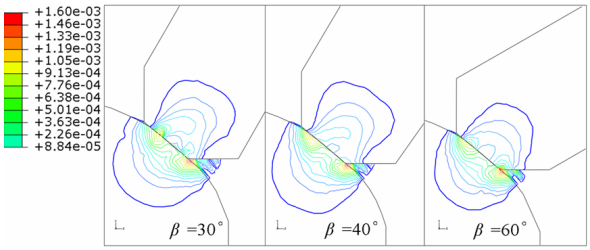

*Impact direction is from right to left

Fig. 9. Damage contour for different disc obliquities under initial impact velocity 3 m/s.

during the instant impact process was investigated at two ends and the middle position of the contact area to demonstrate the influence of the residual velocity on the stop valve. The results at A, B, and C positions are shown in Fig. 6. Fig. 6 illustrates that the residual velocities decreased with increasing impact time. This finding demonstrated that the instant impact energy was gradually absorbed by the valve. Furthermore, Fig. 6 shows that the residual velocity at $\beta = 60°$ varied remarkably corresponding to the results at $\beta = 30°$ and 40°. This finding was attributed to the inertia force of the disc that significantly suppress the rebound effect at $\beta = 30°$ and 40° during the downward movement of the valve. Fig. 6 also illustrates that the maximum fluctuation amplitudes of the residual velocity at $\beta = 60°$ were 1.6 m/s (at A position), 1 m/s (at B position), and 1 m/s (at C position) before 0.02 ms. These conditions led to the huge strain deformation of the valve to dissipate the residual kinetic energy. In particular, for the configuration with the valve disc obliquity $\beta = 60°$, the significant damage was generated at A position.

An in-depth understanding of the influence of the instant impact between the valve disc and the valve seat was obtained by using stress triaxiality ratio σ^*. The results are illustrated in Fig. 7. $\sigma^* < 0$ and $\sigma^* > 0$ represents the compression stress and tension stress, respectively. Fig. 7 illustrates that σ^* at C positions displayed the alternating stress for the valve disc obliquity $\beta = 60°$. The combination of Eqs. (5) and (6) suggested that the tension stress was more detrimental than compression stress. The stress triaxiality ratio that fluctuated most intensively for the obliquity $\beta = 60°$ further demonstrated that the remarkable damage was generated at A and C positions.

Further analysis on the contact stress (Fig. 8) associated with the instant impact between the valve disc and the valve seat was performed at A position to demonstrate the influence of the valve disc obliquity on the instant impact. Fig. 8 illustrates that the contact stress at $\beta = 60°$ maintained the minimum before 0.015 ms. Subsequently, the contact stress at $\beta = 60°$ sharply increased and kept the maximum values after 0.015 ms. Furthermore, the contact stress at $\beta = 60°$ significantly fluctuated, and the maximum amplitude reached 1.65 E + 08 Pa. For the configuration with the valve disc obliquity $\beta = 30°$, the fluctuation amplitude of the contact stress maintained the stable variation. The minimum contact stress was exhibited at $\beta = 40°$.

Accordingly, Fig. 9 shows the damage distribution at 0.05 ms after the onset of the impact for different disc obliquities. Both the disc and the seat had impact damage concentrated in the contact area with maximum damage value above 0.0016, whereas the contact area of the disc was much less damaged or remains undamaged compared with that of the seat. No bulge area was numerically predicted for all kinds of impacted disc. The disc with the initial obliquity $\beta = 40°$ showed minimum impact damage in the contact area among the three geometries. Although all the valve seats showed two moderately large damaged regions, the damage of the seat under disc obliquity $\beta = 40°$ was well distributed. A remarkable rest part remained undamaged for both the disc and the seat.

3.2 Effect of the contact area ratio

The asymmetric disturbance of the impact can be studied

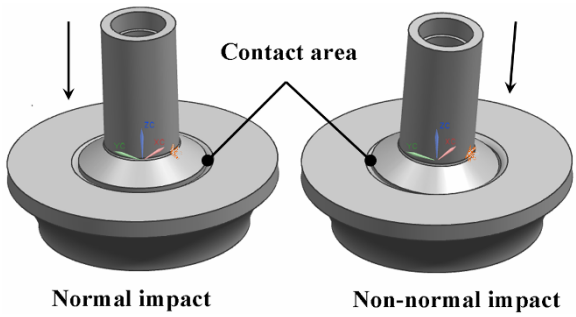

Fig. 10. Contact area of normal and non-normal impact.

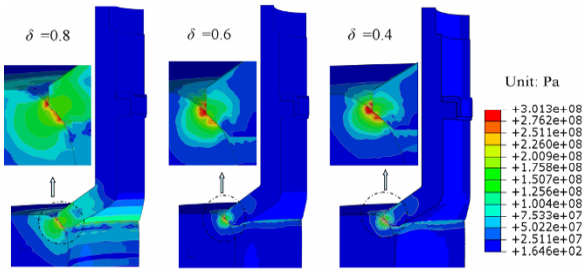

Fig. 11. Distribution of equivalent stress for different contact area ratio under v = 3 m/s.

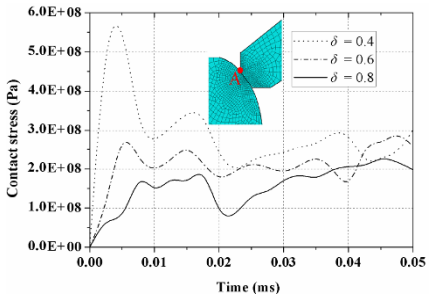

Fig. 12. Effect of contact area ratio on the contact stress–time history plot at position of significant damage.

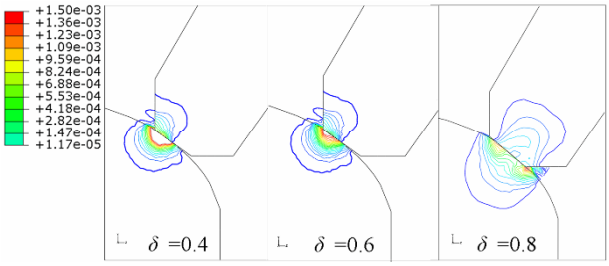

Fig. 13. Damage contour for different contact area ratio under v = 3 m/s.

with the contact area ratio, δ. In this paper, the contact area ratio was defined by the ratio of the contact area under normal impact to the contact area under non-normal impact, which is depicted in Fig. 10. Accordingly, the most severely damaged sections were chosen for comparison. Overall illustration on σ_{eq} distribution at δ = 0.4, 0.6, and 0.8 is shown in Fig. 11. Fig. 11 illustrates that the maximum σ_{eq} gradually moved to the top of the contact area with decreasing δ. Furthermore, the decreasing δ led to the decreasing contact area. In particular, the contact area at δ = 0.4 was only three-fifth of the contact area at δ = 0.8. In addition, the zone of concentrated stress intensively enlarged because of the decreasing δ. The maximum σ_{eq} reached 301.3 MPa at δ = 0.4. Further analysis of δ influencing the contact stress was performed by comparing the time-dependent contact stresses among the three typical contact area ratios. The δ ranges from 0 to 1. The δ = 0 occurs in most severe case of the non-normal impact, and δ = 1 indicates normal impact.

According to operational practice, the starting point of the contact zone usually bears the most severe impact damage partly because of the quick closing and high leak tightness requirement in the valve design. In this case, the starting point of the contact zone was taken as a "representative" position for analysis. Fig. 12 demonstrates that the contact stresses arrived at a high level as soon as the disc impacted the seat. The first peak of the contact stresses ascended within the first 0.01 ms. The contact stresses reduced to a low level with the time increasing. Meanwhile, these contact stresses fluctuated slightly to a stable level. Fig. 12 indicates that the more the contact area ratio δ was, the less the contact stress transiently reached. The contact stress augmented significantly with the δ instantly reducing because the disc critically deviated from the normal impact. Furthermore, Fig. 12 indicates that the highest value of the contact stress for δ = 0.4 reached 588 MPa, which exceeded the yield stress. Although the highest contact stress occurred for δ = 0.4 immediately after the contact, the gap among the three contact stress for δ = 0.4, 0.6, 0.8 decreased gradually with the time increasing. Some of the reasons were connected to the plastic deformation and heat dissipation, which referred to the Eqs. (8) and (9).

To analyze quantitatively the influence of the instant impact on the component, the significant damage was chosen for study, as illustrated in Fig. 13. Fig. 13 illustrates that any deviation from normal impact resulted in a shift on damage concentration and distribution alteration. Furthermore, Fig. 13 numerically predicts the impact damages mainly concentrated on the valve seat for the three cases, while the impact velocity was kept constant at 3 m/s. Fig. 13 indicates that the highly damaged region enlarged with the δ decreasing because of the impact biased toward severely damaged region. The impact of the disc under δ = 0.4 clearly induced huge accumulated damaged region that concentrated on the starting impact point, and the most severe damage was above 0.0015. According to the preceding results, nearly 30% of the damaged area would be completely broken if the impact was continuously performed for a thousand times.

3.3 Effect of the aspect ratio

Given that height, H, and diameter, D, are two structurally related parameters that are usually considered in valve disc design, the dimensionless aspect ratio combines the effects of

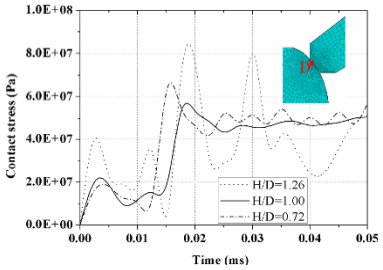

Fig. 14. Effect of aspect ratio on the contact stress–time history plot under v = 3 m/s.

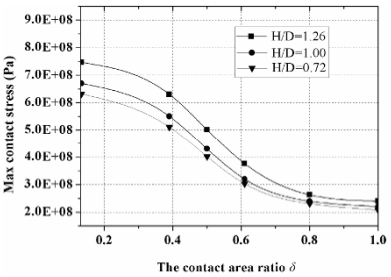

Fig. 15. Max contact stress changes with the contact area ratio for different aspect ratios.

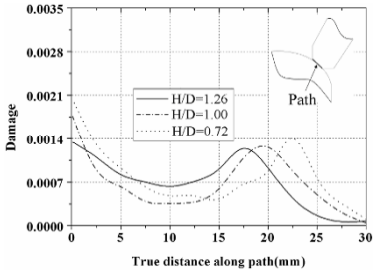

Fig. 16. Effect of the aspect ratio on the impact damage along contact path under v = 3 m/s.

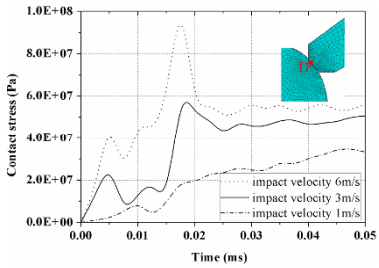

Fig. 17. Comparison of the computed time histories of the contact stress under different impact velocities.

H and D on the impact and can be defined by the form of H/D. The effect of the aspect ratio on the contact stress was analyzed for three valve discs at a position of significant damage, as shown in Fig. 14. Fig. 14 illustrates that the critical fluctuation occurred at around 0.02 ms, and then the fluctuation on the contact stresses returned to a relatively stable level for the three cases. Moreover, the contact stress fluctuated most sharply for the disc with H/D = 1.26, whereas the contact stress under H/D = 0.72 had the highest frequency fluctuation. Fig. 14 also illustrates that the contact stress under H/D = 1 seemed to be more stable than that of the others after 0.02 ms. In addition, Fig. 14 indicates that the highest value at point D appeared slightly later than that at point A (shown in Fig. 12) during the contact stress history. Moreover, the highest contact stress reached 825 MPa for the disc with H/D = 1.26. The mean contact stress for three cases was 430 MPa in the range of 0.02 ms to 0.05 ms.

Further investigation on the max contact stress was performed to look into the effect of the aspect ratio on the max contact stress with varying δ, as shown in Fig. 15. It demonstrated that the max contact stress slightly increased with the increase of the aspect ratio H/D because of the mass alteration by altering the H/D. In particular, when the δ surpassed 0.8, the aspect ratio did not cause any significant change on the max contact stress. However, the effect of the aspect ratio became more notable on max contact stress with reducing δ. The aspect ratio was usually related to the mass. Thus, altering the aspect ratio may lead to a very different distribution on impact damage. The quantitative analysis of the aspect ratio effect on impact damage is presented. One section was chosen for analysis, as shown in Fig. 16. The most severe damage occurred at the starting point of the contact zone, and the second peak of the impact damage shifted away from the starting point with the increase of the aspect ratio. Compared with the impact damage under other values of H/D, the impact damage under H/D = 1 distributed more reasonably because of its minimum total damage within the contact path.

3.4 Effect of the impact velocity

In this study, the effect of the impact velocity on the impact was investigated at a typical damaged point D. Point D was chosen because the behaviors of another point should be determined, and the illustration at point A was already detailed in the preceding sections. Fig. 17 illustrates that the impact velocity significantly influenced the contact stress. Fig. 17 also illustrates that the increasing impact velocity led to the significant increase in the contact stress. The contact stress at the impact velocity 6 m/s increased significantly corresponding to the results at the impact velocity 3 m/s and 1 m/s before 0.02 ms, and a distinctive peak of the contact stress could not be determined through 0.05 ms for the impact velocity 1 m/s. Furthermore, the contact stress did not occur immediately after the impact because of the corresponding impact position (point D) away from the starting point (point A). Thus, the impact damage at point D would be greatly different from that at point A. In addition, Fig. 17 indicates that the highest peaks of the contact stresses at the impact velocities 6 m/s and 3 m/s were 96 MPa and 58 MPa, respectively, at 0.018 ms, and the contact stress at the impact velocity 1 m/s reached the highest value of 31.5 MPa at 0.05 ms.

An examination on the max contact stress was conducted to

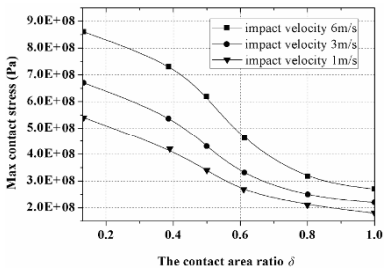

Fig. 18. Max contact stress changes with the contact area ratio under different impact velocities.

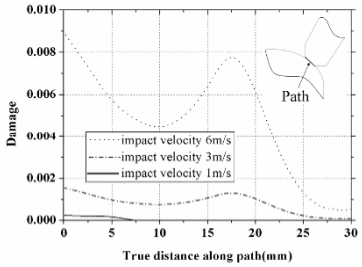

Fig. 19. Effect of impact velocity on the impact damage along contact path.

investigate the effect of the impact velocity on the max contact stress with varying δ. This examination indicated that the max contact stress was sensitive to the impact velocity, and the max contact stress nonlinearly increased with increasing the impact velocity. Fig. 18 illustrates that the max contact stress decreased with increasing δ and increased with increasing the impact velocity under the same δ. The highest value of max contact stress surpassed 800 MPa, which was beyond the initial yield stress of the material. In addition, the impact velocity 6 m/s led to a 20% increase on max contact stress compared with the results at impact velocity 3 m/s. Furthermore, the high impact velocity was unsuitable for the low δ state in the valve application. The $\delta = 0.8$ seemed a threshold value. Once the contact area ratio δ exceeded the threshold value, the effect of the impact velocity on the max contact stress would be significantly enlarged.

However, the impact velocity also influenced the impact damage. The results are shown in Fig. 19. Fig. 19 indicates that the impact damage was very sensitive to the impact velocity. This finding could be further proved by the comparison between Figs. 16 and 19. Moreover, high impact velocity led to huge impact damage that was fatal for the application in the turbine valve. The impact damage at the impact velocity 6 m/s was more than two times of the result at the impact velocity 3 m/s. The impact damage profile in Fig. 19 resembles the results in Fig. 16. However, Fig. 19 illustrates that the impact damage is insignificant for the impact velocity below 1 m/s except slight damage at the starting region of the contact zone.

4. Conclusions

This study described a coupled computational model of viscoplasticity and damage, which can predict dynamic response and impact damage during impact. Based on this theoretical approach, the dynamic response and impact damage of the valve disc against the seat was investigated by using commercial code ABAQUS augmented by a user-defined material subroutine. The effects of the variation of selected design parameters on the damage of the valve were analyzed in terms of contact stress, Von Mises stress, max contact force, triaxiality factor, and impact damage. Three key points are presented as follows:

(1) Numerical calculations demonstrated that the initial valve disc should be obliquity $\beta = 40°$. This disc obliquity avoided stress concentration that could lead to further impact damage. The high impact damage concentrated on the two spots, one of which was at the starting point of the contact zone. In addition, the residual velocity of the position decreased rapidly, which further proved that this position suffered significant damage caused by the impact.

(2) Given that the variation of the contact area ratio δ remarkably affected the final impact damage and dynamic response, robustness and precision are highly required for the valve shutdown operation, because any deviation from normal impact would induce low δ that resulted in high contact stress and impact damage.

(3) The contact stress increased with impact velocity and the aspect ratio. Furthermore, the impact damage was more sensitive to the impact velocity than it was to the aspect ratio. The increase in the contact stress at high impact velocity was more rapid than that at low impact velocity. The valve disc with 97.81 kg, H/D = 1, and the impact velocity 1 m/s had the lowest impact damage and possessed the most stable dynamic properties among the three cases.

Acknowledgment

This work is supported by the Provincial Youth Fund (No. Q15E050024), Key Project of Chinese Ministry of Education (No. 309012), and Research Project of State Key Laboratory of Mechanical System and Vibration (No. MSV201115).

References

[1] S. K. Dawawala, Design of throttle valve for BB34/034, *Design Report DE-87019*, 2 (1987).

[2] R. Swanekamp, *Forcus on O&M of valves*, Power, March/April (1998).

[3] Z. Mazur, R. Campos-Amezcua, G. Urquiza-Beltrán and A. García-Gutiérrez, Numerical 3D simulation of the erosion due to solid particle impact in the main stop valve of a steam turbine, *Appl. Therm. Engng.*, 24 (13) (2004) 1877-1891.

[4] Z. B. Chen, G. Q. Li, H. Zhang and C. Y. Chen, Fatigue life prediction of regulating valves on the intermediate-pressure section of a 400 MW steam turbine, *Engng. Fail. Analysis*, 16 (5) (2009) 1483-1492.

[5] Z. Z. Peng, Z. S. Ding and Z. Q. Wang, Three-dimensional

transient temperature field of the valve body of a turbine regulating valve and the analysis of its stress field, *J. Engng. Therm. Energy Pow.*, 17 (1) (2002) 80-83.

[6] M. Klaus, H. G. Reimerdes and N. K. Gupta, Experiental and numerical investigations of residual strength after impact of sandwich panels, *Int. J. Impact Engng.*, 44 (2012) 50-58.

[7] T. Borvik, O. S. Hopperstad, T. Berstad and M. Langseth, Numerical simulation of plugging failure in ballistic penetration, *Int. J. solids struct.*, 38 (2001) 6241-6264.

[8] Bonora et al., CDM modeling of ductile failure in ferritic steels: assessment of the geometry transferability of model parameters, *Int. J. Plasticity*, 22 (2006) 2015-2047.

[9] S. Chandrakanth and P. C. Pandey, An isotropic damage model for ductile material, *Engng Fract. Mech*., 50 (1995) 457-465.

[10] G. G. Corbett, S. R. Reid and W. Johnson, Impact loading of plates and shells by free-flying projectiles: a review, *Int. J. Impact Engng.*, 18 (1996) 141-230.

[11] W. Goldsmith and S. A. Finnegan, Normal and oblique impact of cylindro-conical and cylindrical projectiles on metallic plates, *Int. J. Impact Engng*, 4 (2) (1986) 83-105.

[12] J. Lemaitre, Formulation and identification of damage kinetic constitutive equations in: D. Krajcinovic, *Continuum Damage Mechanics Theory & Application*, Springer-Verlag, Wien-NewYork (1990).

[13] Z. X. Lin, F. F. Jiang and Y. Q. Tang, Multi-scale analyses on seismic damage and progressive failure of steel structures, *Finit. Elem. Anal. Des.*, 48 (2012) 1358-1369.

[14] G. R. Johnson and W. H. Cook, Fracture characteristics of three metals subjected to various strains, strain rates, temperatures and pressures, *Engng. Fract. Mech.*, 21 (1) (1985) 31-48.

[15] O. S. Hopperstad, T. Berstad, T. Børvik and M. Langseth, A computational model of visco-plasticity and ductile damage, *Proceedings of Fifth International LS-DYNA users Conference*, Michigan, USA, September 21-22 (1998a).

[16] T. Børvik, M. Langseth, O. S. Hopperstad and K. A. Malo, Ballistic penetration of steel plates, *Int. J. Impact Engng.*, 22 (1999) 855-886.

[17] T. Børvik, O. S. Hopperstad, T. Berstad and M. Langseth, Perforation of 12 mm thick steel plates by 20 mm diameter projectiles with flat, hemispherical and conical noses: Part II: numerical simulations, *Int. J. Impact Engng.*, 27 (1) (2002) 37-64.

[18] P. Rosakis, A. J. Rosakis, G. Ravichandran and J. Hodowany, A thermodynamic internal variable model for the partition of plastic work into heat and stored energy in metals, *J. Mech. Phys. Solids*, 48 (2000) 581-607.

[19] Y. Bai and B. Dodd. *Adiabatic shear Localization: occurrence, theories and applications*, Oxford: Pergamon Press (1992).

[20] D. Samantaray, S. Mandal and A. K. Bhaduri, A comparative study on Johnson Cook modified Zerilli- Armstrong and Arrhenius-type constitutive models to predict elevated temperature flow behavior in modified 9Cr-1Mo steel, *Comput. Mater. Sci.*, 47 (2009) 568-576.

[21] S. R. Chen and T. George Gray III, Constitutive behavior of tantalum and tantalum-tungsten alloys, *Metall. Mater. Trans. A*, 27 (1996) 2994-3006.

[22] J. Lemaitre and R. Desmorat, *Engineering damage mechanics*, Springer-Verlag (2005).

[23] I. Rohr, H. Nahme and K. Thoma, Material characterization and constitutive modeling of ductile high strength steel for a wide range of strain rates, *Int. J. Impact Engng.*, 31 (2005) 401-433.

Mao Jianfeng, a lecturer in the College of Mechanical Engineering at ZheJiang University of Technology, Hangzhou, China, holds a doctor of philosophy degree from Shanghai Jiaotong University. His research interests include high-temperature structural integrity and chemical–mechanical system.

Wang Weizhe is an associate professor in the School of Mechanical Engineering, Shanghai Jiao Tong University, China. His research interests focus on the structural analysis of high-temperature components and constitutive models.